Ferroelectricity of wurtzite Al$_{1-x}$Hf$_x$N heterovalent alloys
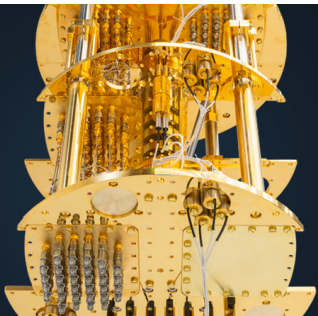
Nate S. P. Bernstein ; Daniel Drury ; Cheng-Wei Lee ; Tatau Shimada ; Yuki Sakai ;
Oliver Rehm ; Lutz Baumgarten ; Martina Müller ; Prashun Gorai ; Yoshiki Iwazaki ; Glen R. Fox ;
Keisuke Yazawa ; Brendan Hanrahan ; Geoff L. Brennecka ✉

Check for updates

CHORUS

View Online

Export Citation

AIP Publishing

Ferroelectricity of wurtzite $Al_{1-x}Hf_xN$ heterovalent alloys

View Online   Export Citation   CrossMark

Nate S. P. Bernstein,[1,a)] (iD) Daniel Drury,[2] (iD) Cheng-Wei Lee,[1] (iD) Tatau Shimada,[3] (iD) Yuki Sakai,[3] (iD) Oliver Rehm,[4] (iD)
Lutz Baumgarten,[5] (iD) Martina Müller,[4] (iD) Prashun Gorai,[1,6] (iD) Yoshiki Iwazaki,[3] (iD) Glen R. Fox,[7] (iD)
Keisuke Yazawa,[1,8] (iD) Brendan Hanrahan,[2] (iD) and Geoff L. Brennecka[1,b)] (iD)

AFFILIATIONS

[1]Department of Metallurgical and Materials Engineering, Colorado School of Mines, Golden, Colorado 80401, USA
[2]U.S. Army Combat Capabilities Development Command-Army Research Laboratory, Adelphi, Maryland 20783, USA
[3]TAIYO YUDEN CO., LTD., 2-7-19, Kyobashi, Chuo-ku, Tokyo 104-0031, Japan
[4]Department of Physics, Universität Konstanz, D-78457 Konstanz, Germany
[5]Forschungszentrum Jülich GmbH, Peter Grünberg Institut (PGI-6), D-52425 Jülich, Germany
[6]Department of Chemical and Biological Engineering, Rensselaer Polytechnic Institute, Troy, New York 12180, USA
[7]Fox Materials Consulting, LLC, Colorado Springs, Colorado 80908, USA
[8]Materials Science Center, National Renewable Energy Laboratory, Golden, Colorado 80401, USA

a)Electronic mail: nbernstein@mines.edu
b)Author to whom correspondence should be addressed: gbrennec@mines.edu

ABSTRACT

Thin films of aluminum hafnium nitride ($Al_{1-x}Hf_xN$) were synthesized via reactive magnetron sputtering for Hf contents up to $x = 0.13$. X-ray diffraction showed a single c-axis oriented wurtzite phase for all films. Hard x-ray photoelectron spectroscopy demonstrated homogeneous Al:Hf distribution through the thin films and confirmed their insulating character. A collection of complementary tests showed unambiguous polarization inversion, and thus ferroelectricity in multiple samples. Current density vs electric field hysteresis measurements showed distinct ferroelectric switching current peaks, the piezoelectric coefficient $d_{33,f,meas}$ measured using a double beam laser interferometer (DBLI) showed a reversal in sign with similar magnitude, and anisotropic wet etching confirmed field-induced polarization inversion. This demonstrates the possibility of using tetravalent–and not just trivalent–alloying elements to enable ferroelectricity in AlN-based thin films, highlighting the compositional flexibility of ferroelectricity in wurtzites and greatly expanding the chemistries that can be considered for future devices.

Ternary wurtzite-type aluminum nitride-based thin films ($Al_{1-x}M_xN$) have gained recent attention directed at applications utilizing their ferroelectric (FE) behavior. These applications include, among others, high-operating temperature, nonvolatile, random-access memory (HOT-NVM),[1] and ferroelectric high electron mobility transistors (Fe-HEMTs).[2,3] To date, the following $Al_{1-x}M_xN$ ferroelectric thin films have been reported: $Al_{1-x}Sc_xN$,[4] $Al_{1-x}B_xN$,[5] $Al_{1-x}Y_xN$,[6] and $Al_{1-x}Gd_xN$.[7] Note that the M-element in all cases is nominally trivalent, a logical approach to replace the Al^{3+} cation.

The conventional expectation is that percent-level additions of a non-trivalent M-element could introduce sufficiently high free carrier concentrations to lead to metallic conduction. In this work, we demonstrate that sputtered thin films of $Al_{1-x}Hf_xN$ are electrical insulators and can be ferroelectric up to at least $x = 0.13$. To date, this is the first $Al_{1-x}M_xN$ thin film showing ferroelectricity with heterovalent M-element alloying. Importantly, this work shows that researchers working on HOT-NVM and FE-HEMTs are not limited to trivalent cation replacements, thus increasing compositional options for AlN-based ferroelectric films and driving deeper studies of charge balancing defect compensation in III-N alloys.

A charge-balancing approach has also dominated the more extensive alloying efforts across the piezoelectric thin film community,

including both direct substitution of Al^{3+} by other trivalent species and stoichiometric combinations of multiple alloying species.[8] Such multivalent alloy studies started with computational work from Iwazaki[9] and Tholander,[10] and Akiyama and coworkers have consistently led the community's experimental efforts, including key studies on $Al_{1-x}(Mg,Nb)_xN$,[11] $Al_{1-x}Mg_{x/2}Ti_{x/2}N$,[12] $Al_{1-x}(Mg,Ta)_xN$,[13] and $Al_{1-x}Mg_{x/2}Hf_{x/2}N$.[14] It is worth noting that Uehara's $Al_{1-x}(Mg,Nb)_xN$ study reported the greatest piezoelectric response in films with Mg/Nb ratios that would not correspond to an effective average valence of 3+ for pure Mg^{2+} and Nb^{5+}, but they did see evidence for multivalency in the Nb species.[11]

Studies on intentionally heterovalent alloys such as $Al_{1-x}Mg_xN$,[15] $Al_{1-x}Si_xN$,[16] and even $Al(O,N)$[17,18] suggest some degree of control over growth polarity. However, the focus of these reports has primarily been on piezoelectric properties, with only the report by Islam et $al.$ discussing polarization reversal and leakage current.[18] Reports of $Al_{1-x}Sc_xN$ remaining electrically insulating[17] and even ferroelectric with an approximate oxygen content of 4 at.%[18,19] suggest value in exploring other donor dopants. DFT calculations of the piezoelectric response also motivate the study of $Al_{1-x}Hf_xN$[20] and heterovalent AlN-based alloys more broadly.

Thin films of $Al_{1-x}Hf_xN$ were synthesized using reactive magnetron sputtering techniques similar to previous studies.[1,21,22] Primary samples were deposited on (001) 4H-SiC substrates with sputtered continuous molybdenum bottom and top electrodes ($Mo/Al_{1-x}Hf_xN/Mo/SiC$); this stack was chosen because of its relevance to high-temperature electronics. The top electrodes were all circular and varied in diameter from 50 to 125 μm. Top electrode patterning was done with wet etching and a photolithographic liftoff process. Three sputter targets were used: Mo (99.95 % Kurt J Lesker Co.), Al (99.999 %, Kurt J Lesker Co.), and Hf (99.9 % Stanford Advanced Materials). Targets were 10.16 cm in diameter. The Hf target purity was 99.5 % when including Zr as a contaminant (i.e., Zr < 0.5 %). Two samples of $Al_{1-x}Hf_xN$ were grown by varying the Hf target RF power while maintaining a constant Al target pulsed DC power to control the Al/Hf cation ratio (see Table I). One sample of AlN was grown in the same series to compare these films with previous work. The nitride layer of all three thin film stacks was sputtered with the following conditions: 2 mTorr of Ar/N_2 (40/40 sccm flow), a substrate heater set point of 400 °C, and a deposition time of 100 min. The Hf content listed in Table I was measured using Rutherford backscattering spectrometry (RBS) made by National Electrostatics Corp. Elements other than Hf, Al, Mo, Zr, and Si were all below the detection threshold of the RBS instrument. Complementary samples for beamline measurements were deposited on AlN-seeded sputtered continuous molybdenum bottom electrodes on Si wafers. Additional preparation and synthesis details are provided in the supplementary material.

TABLE I. Deposition conditions and film properties.

| Hf power density (W/cm²)	Total Dep. rate (nm/min)	Hf cation content (cat. %)	Film thickness (nm)
0.0	1.8	0	180
11.8	2.0	6	200
17.7	2.2	13	220

Figures 1(a) and 1(b) show θ–2θ scans and ω-rocking curves, respectively (using a Panalytical X'Pert3 MRD XL diffractometer), on c-axis textured single-phase wurtzite films. No diffraction peaks originating from anomalously oriented grains (AOGs) were observed. Figure 1(b) shows a full width half max (FWHM) range of 1.2°–1.4°, which is similar to—or better than—previously reported FWHM values for sputtered ferroelectric nitrides.[22–24] Additional diffraction data, including lattice parameters, are shown in the supplementary material.

Figure 2 shows the valence band electronic structure determined by hard x-ray photoelectron spectroscopy (HAXPES)[25,26] of $Al_{1-x}Hf_xN$ films with varying stoichiometry (nominally $x = 0.05$ and 0.09). Figure 2(a) shows core-level spectra of N 1s, Hf $4p_{3/2}$, and Al 2s acquired at 6 keV (bulk-sensitive to a depth of $\sim$18 nm) and 2.8 keV (surface-sensitive to a depth of $\sim$9 nm). The strong agreement between the theoretical and measured 2.8 keV spectra for Hf $4p_{3/2}$ and Al 2s suggests a homogeneous distribution of Hf and Al throughout the $Al_{1-x}Hf_xN$ layer. The measured N 1s intensity at 2.8 keV is lower than predicted, indicating a nitrogen deficiency at the surface, likely due to oxidation in uncapped samples. Figure 2(b) displays valence band (VB) spectra of $Al_{1-x}Hf_x$ N films with different Hf contents, measured using 6 keV photons. Increasing Hf content results in a noticeable shift of the valence band maximum toward the Fermi level, reducing the valence band offset (VBO) relative to AlN from 3.7 eV to 2.7 eV for $Al_{0.91}Hf_{0.09}N$, as schematically depicted in Fig. 2(c). A nonmetallic character is indicated for all three $Al_{1-x}Hf_xN$ samples. Additional details on HAXPES experiments and data analysis are given in the supplementary material.

Figure 3 shows the results of electrical measurements. For all measurements in this Letter, a positive E-field direction is defined as pointing from the bottom electrode to the top electrode, normal to the substrate. Figures 3(a) and 3(b) show unambiguous ferroelectric switching current peaks. Data in Figs. 3(a) and 3(b) were collected by applying a triangular wave to the samples at 10 kHz, using a tester from Radiant Technologies, Inc. From these data, a value of coercive electric field (E_c) was extracted at ±5.5 and ±4.7 MV/cm for $x = 0.06$ and 0.13, respectively, based on the switching current peak. These data showed comparable magnitude and the same trend of both E_c and crystallographic u-parameter vs x as other ferroelectric nitrides: increasing M-element atomic fraction results in decreased u and E_c.[4,5,27–31] Large and variable leakage current values under high field pulses hindered attempts to quantitatively separate switching and leakage current contributions via Positive Up Negative Down (PUND) and related measurements. See the supplementary material for further details.

Figure 3(c) shows that at low applied E-field, the $x = 0.06$ and 0.13 samples were more insulating than typical ferroelectric $Al_{0.7}Sc_{0.3}N$ films.[1] Data in Fig. 3(c) were taken using a Keithley 4200A-SCS. Polarization vs applied E-field (P–E) loops are shown in 3(d) at 50 kHz (see the supplementary material for 10 kHz loops). The top electrode diameter used was 50 μm for all measurements shown in Fig. 3 and was connected to the signal ground for all tests. Figure S3(c) shows that the relative permittivity (ε_r) is comparable to other Al_{1-x} M_xN wurtzites.[5,32]

To support the claim that the current density peaks in Figs. 3(a) and 3(b) were due to ferroelectricity, further measurements were carried out using small signal d_{33} testing. The first part of this measurement employed multiple voltage pulses applied to the Mo top

09 December 2025 14:40:56
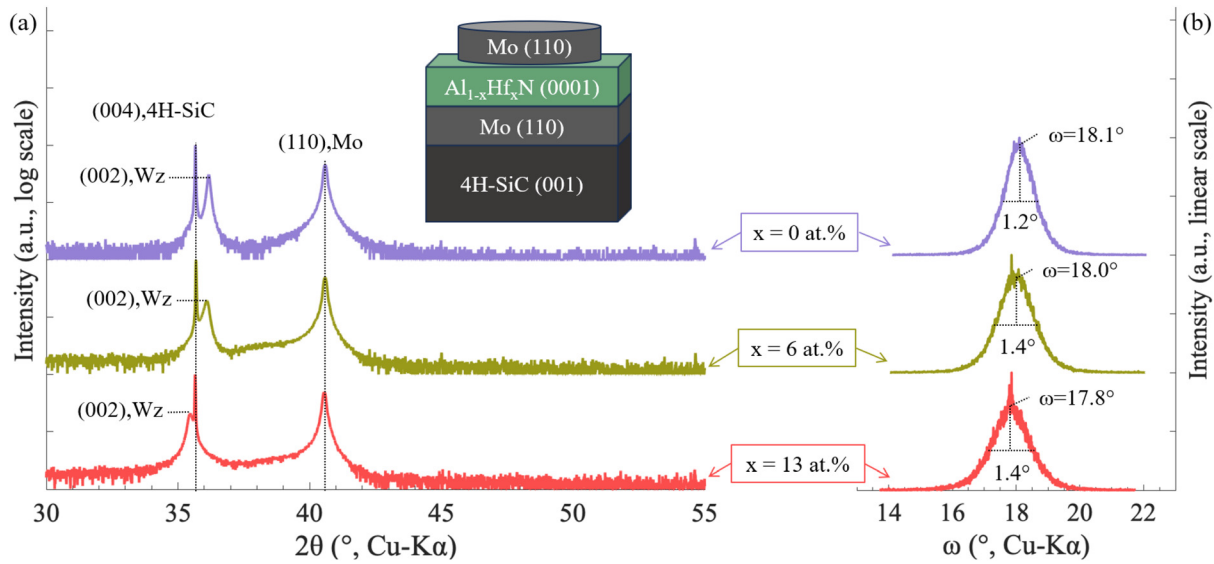
FIG. 1. X-ray diffraction: (a) θ–2θ scans show peaks from the substrate, electrode, and (002), Wz exclusively, indicating that the films were single-phase wurtzite. (b) The ω-rocking curves measured around the (002), Wz peaks show that the films were well textured. Hf cation atomic percentages were measured with RBS.
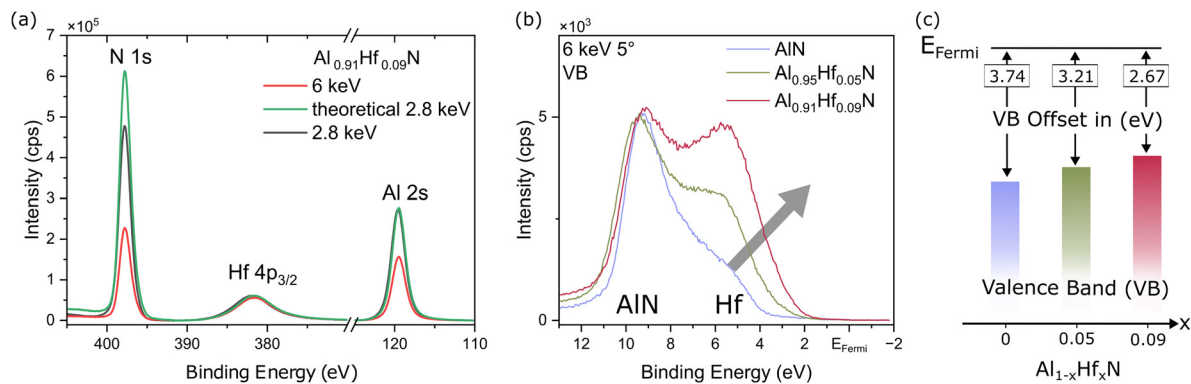
FIG. 2. HAXPES measurement of $Al_{1-x}Hf_xN$ films. (a) Core-level spectra of $Al_{0.91}Hf_{0.09}N$ measured at 6 and 2.8 keV, indicating a homogeneous Al:Hf distribution. (b) and (c) Valence band spectra measured at 6 keV, comparing AlN, $Al_{0.95}Hf_{0.05}N$, and $Al_{0.91}Hf_{0.09}N$. A reduced valence band offset (VBO) is observed with increasing Hf incorporation; however, a non-metallic character is maintained for all Hf concentrations.

electrodes on the $x = 0.06$ and 0.13 films to ensure that the film region beneath the electrodes was fully switched into the N-polar state. Then, a small signal sinusoidal E-field was applied to the films with a frequency of 200 Hz and an amplitude of 0.5 MV/cm (E_{ss}). The DBLI was then used to obtain the as-measured value of the piezoelectric coefficient: $d_{33,f,meas}$. The magnitude of $d_{33,f,meas}$ is shown in Fig. 4(e). Figure 4(e) also shows $d_{33,calc}$ values calculated using density functional theory (DFT). The $d_{33,f,meas}$ values increase up to 12 pm/V at $x = 0.13$, and the qualitative trend for calculation and measurement matched. Note that the absolute value is not quantitatively comparable between DFT and experimental results since DFT calculations are performed assuming single crystals, and $d_{33,f,meas}$ is affected by clamping.[33]

After the switching pulse and subsequent measurement of $d_{33,f,meas}$, a bias electric field was applied to the films as a staircase function superimposed with E_{ss} (see the supplementary material for an

illustration of the function). Figures 4(c) and 4(d) show the result of this measurement for films with $x = 0.13$ and 0.06, respectively. The respective films switched from N-polar to M-polar upon exceeding the bias field needed to switch, as illustrated by labels indicating film polarity in Fig. 4(d). The magnitude of each measurement step was 0.1 MV/cm. The dwell time after each step in voltage was 5 s, allowing for 1000 averages of E_{ss} to occur. This averaging was necessary for extracting the angstrom-level field-induced displacement. A total of 160 points were collected, and therefore the loop period of the measurements in Figs. 4(c) and 4(d) was 800s.

The reduced E_c observed in Figs. 4(c) and 4(d) relative to Fig. 3(b) is attributed to the increased applied E-field period of the measurement:[34] 100 μs for Fig. 3(b) vs 800s for Figs. 4(c) and 4(d). As the applied bias E-field was cycled, an unambiguous change occurred in the sign of $d_{33,f,meas}$ and $\phi_{33,f,meas}$ shifted from 0° to 180°, indicating
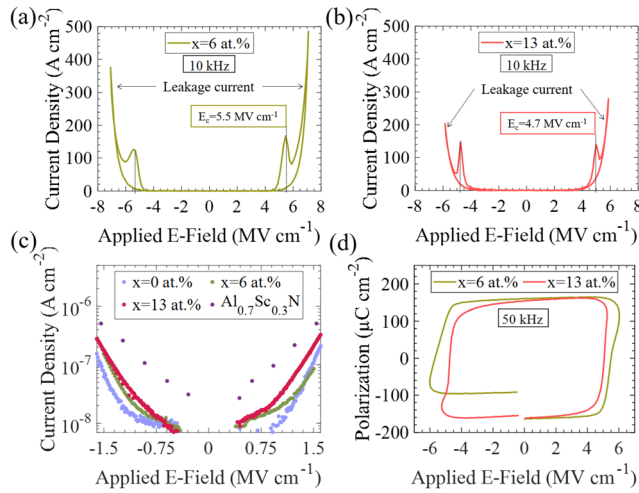
FIG. 3. Electrical measurements showed FE switching for films with $x = 0.06$ and $x = 0.13$. (a) and (b) Hysteresis measurements of current density vs applied E-field showed FE switching for films with $x = 0.06$ and $x = 0.13$, respectively. (c) These $x = 0.06$ and $x = 0.13$ films were insulators and had current densities at low E-fields that were lower than those of comparable $Al_{0.7}Sc_{0.3}N$ samples.[1] (d) Polarization vs applied E-field loops at 50 kHz.

polarization inversion occurred. The applied E-field loops shown in Figs. 4(c) and 4(d) corroborate the ferroelectric behavior of these $Al_{1−x}Hf_xN$ films. The decrease in $d_{33,f,meas}$ when $|E| > 3$ MV/cm and $\phi_{33,f,meas}$ deviating from $0°$ and $180°$ seen in Fig. 4(c) is hypothesized to be due to an increased real component magnitude of the impedance of the sample.

Anisotropic acid etching further confirmed that field-induced polarization reversal occurred. H_3PO_4 was applied to a film where a region had been pulsed metal polar [see Fig. 4(a)]. The step edge of the remnant M-polar region can be seen in Fig. 4(b) while the surrounding as-grown N-polar region was dissolved, since H_3PO_4 dissolves N-polar surfaces faster than M-polar surfaces.[4,35]

Using DFT, we calculated d_{33} as a function of Hf context for $Al_{1−x}Hf_xN$ alloys (see the supplementary material for details). Figure 4(e) shows that the predicted value for pure AlN (5.22 pm/V) is consistent with the previous DFT-based prediction (~ 4–5 pm/V).[9,20] Overall, Hf substitution with charge compensation by Al vacancies increases d_{33}, and the trend of d_{33} vs x qualitatively agrees with the experimental trend, noting again the differences in single-crystal calculations vs clamped thin film measurements.

To clarify the charge compensation mechanism for the typically tetravalent dopant Hf, we calculated defect and carrier concentrations at constant Hf concentration of $10^{21}/cm^3$ ($= 2.1$ at. %) as shown in Fig. 5 (see the supplementary material for details). Under N-rich growth conditions, V_{Al}''' exhibits a low formation energy as described in Fig. S10(a). Consequently, the resultant high concentration of V_{Al}''' almost compensates the positive charge of $Hf_{Al}^{\bullet}$ [see Fig. 5(a)]. On the other hand, the high formation energy of V_{Al}''' under Al-rich growth conditions [Fig. S10(b)] leads to a lower concentration of V_{Al}''', thus resulting in a higher electronic carrier concentration when compared with the N-rich conditions [Fig. 5(b)]. The actual experimental conditions are considered to lie between these N-rich and Al-rich extremes. Therefore, our calculations suggest that the charges carried by Hf_{Al} were partially (mostly) compensated by V_{Al}''', leading to a relatively low electronic carrier concentration and overall insulating character of the $Al_{1−x}Hf_xN$ films.

In summary, this work showed that $Al_{1−x}Hf_xN$ sputtered thin films remain insulating and can be ferroelectric. This was shown via
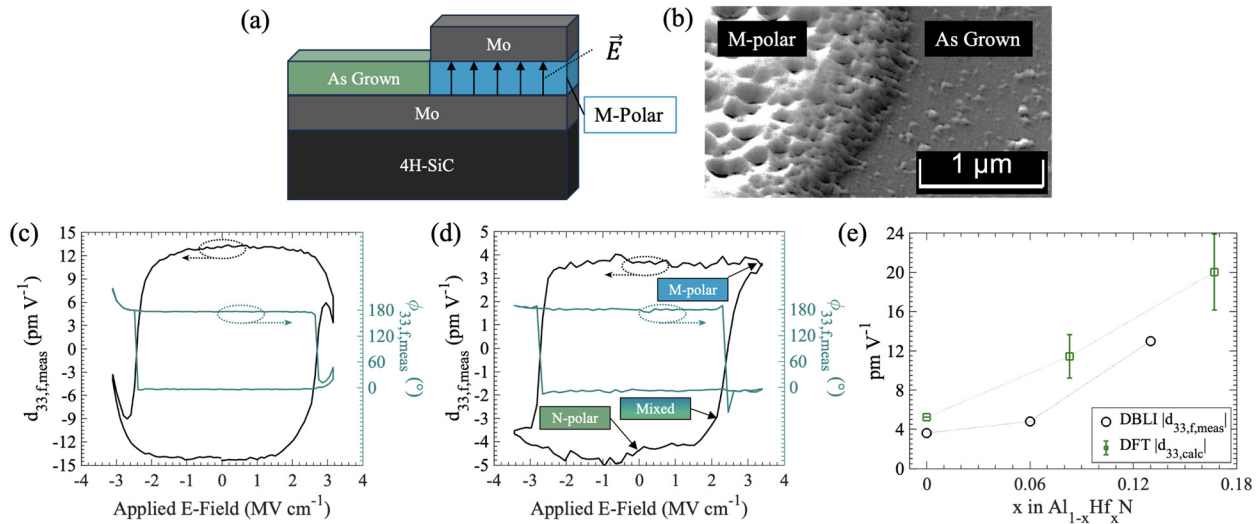
FIG. 4. Polarity inversion confirmed using acid etching and piezoelectric measurements. (a) Film pulsed M-polar. (b) SEM image of the M-polar step edge after etching in 80 °C H_3PO_4. (c) DBLI piezoelectric measurement for $x = 0.13$ film. $\phi_{33,f,meas}$ deviating from $0°$ and $180°$ is hypothesized to be due to leakage current. (d) DBLI measurement for $x = 0.06$ with markers showing the change in polarity of the film around the "staircase" loop. See the supplementary material for more details. (e) Magnitude of the DBLI-measured ($|d_{33,f,meas}|$) and DFT-calculated ($|d_{33,calc}|$) piezoelectric coefficient for zero E-field. Connecting lines between points are a visual aid. (c) and (d), and (e) $|d_{33,f,meas}|$ data were not compensated for substrate clamping effects of the 4H–SiC substrate. The loop period of (c) and (d) was 800 s, leading to a much lower E_c than shown in Figs. 3(a) and 3(b).[34]
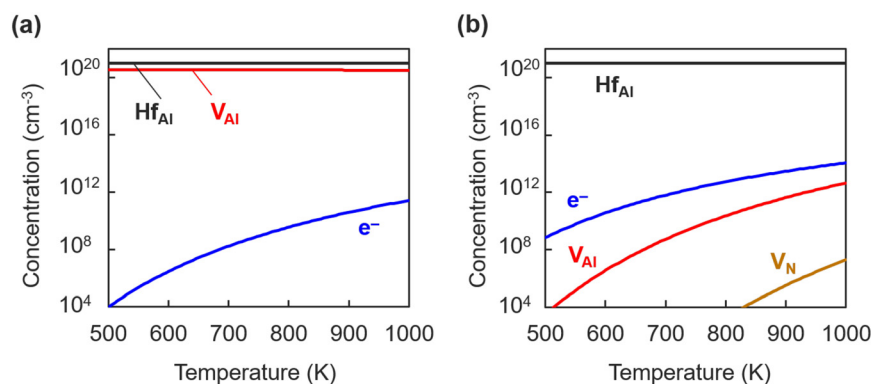
FIG. 5. Carrier and defect concentrations as a function of temperature under (a) N-rich and (b) Al-rich growth conditions.

switching current peaks, small signal $d_{33,f,meas}$ DBLI measurements, and anisotropic etching to confirm polarization inversion. DFT calculations and HAXPES experiments both reinforced the electrical measurement findings that the material system is electrically insulating. While this work did not focus on HOT-NVM or FeHEMTs specifically, this work does enable researchers to think beyond trivalent substitutions when designing devices, opening up more possibilities for better device performance. Future work is planned to identify and quantify specific charge compensation mechanisms and electronic structure for $Al_{1-x}Hf_xN$ with higher fidelity.

See the supplementary material for further measurements and additional method details for all measurements and computations. It also contains spectroscopic ellipsometry and reciprocal space map data.

AUTHOR DECLARATIONS
Conflict of Interest

The authors have no conflicts to disclose.

Author Contributions

Nate S. P. Bernstein: Conceptualization (lead); Data curation (lead); Formal analysis (lead); Investigation (equal); Methodology (lead); Validation (lead); Visualization (lead); Writing – original draft (lead); Writing – review & editing (lead). **Daniel Drury:** Conceptualization (supporting); Formal analysis (supporting); Funding acquisition (equal); Investigation (supporting); Methodology (supporting); Project administration (equal); Resources (equal); Writing – review & editing (supporting). **Cheng-Wei Lee:** Formal analysis (equal); Investigation (equal); Methodology (equal); Writing – original draft (equal); Writing – review & editing (equal). **Tatau Shimada:** Formal analysis (equal); Investigation (equal); Methodology (equal); Writing – original draft (equal); Writing – review & editing (equal). **Yuki Sakai:** Formal analysis (supporting); Investigation (supporting); Methodology (supporting); Writing – original draft (supporting); Writing – review & editing (supporting). **Oliver Rehm:** Formal analysis (equal); Investigation (equal); Methodology (equal); Writing – original draft (equal); Writing – review & editing (equal). **Lutz Baumgarten:** Formal analysis (supporting); Writing – original draft (supporting); Writing – review & editing (supporting). **Martina Müller:** Formal analysis (supporting); Funding acquisition (equal); Writing – original draft (supporting); Writing – review & editing (supporting). **Prashun Gorai:** Writing – original draft (supporting); Writing – review & editing (supporting). **Yoshiki Iwazaki:** Funding acquisition (equal); Writing – review & editing (supporting). **Glen R. Fox:** Formal analysis (supporting); Methodology (supporting); Writing – original draft (supporting); Writing – review & editing (supporting). **Keisuke Yazawa:** Conceptualization (supporting); Formal analysis (equal); Investigation

DATA AVAILABILITY

The data that support the findings of this study are available from the corresponding author upon reasonable request.

REFERENCES

[1] D. Drury, K. Yazawa, A. Zakutayev, B. Hanrahan, and G. Brennecka, Micromachines **13**, 887 (2022).

[2] J. Casamento, K. Nomoto, T. S. Nguyen, H. Lee, C. Savant, L. Li, A. Hickman, T. Maeda, J. Encomendero, V. Gund, A. Lal, J. C. M. Hwang, H. G. Xing, and D. Jena, in *International Electron Devices Meeting (IEDM)* (IEEE, San Francisco, CA, 2022).

[3] J. Casamento, J. Hayden, S. Trolier-McKinstry, J.-P. Maria, T.-S. Nguyen, K. Nomoto, H. G. Xing, and D. Jena, in *Semiconductors and Semimetals, Emerging Ferroelectric Materials and Devices*, edited by J. Heron and Z. Mi (Elsevier, 2023), Vol. 114, pp. 119–136.

[4] S. Fichtner, N. Wolff, F. Lofink, L. Kienle, and B. Wagner, J. Appl. Phys. **125**, 114103 (2019).

[5] J. Hayden, M. D. Hossain, Y. Xiong, K. Ferri, W. Zhu, M. V. Imperatore, N. Giebink, S. Trolier-McKinstry, I. Dabo, and J.-P. Maria, Phys. Rev. Mater. **5**, 044412 (2021).

[6] D. Wang, S. Mondal, J. Liu, M. Hu, P. Wang, S. Yang, D. Wang, Y. Xiao, Y. Wu, T. Ma, and Z. Mi, Appl. Phys. Lett. **123**, 033504 (2023).

[7] C.-W. Lee, R. W. Smaha, G. L. Brennecka, N. M. Haegel, P. Gorai, and K. Yazawa, APL Mater. **13**, 021114 (2025).

[8] E. Thomas and R. Ranjith, ECS Trans. **107**, 15229 (2022).

[9] Y. Iwazaki, T. Yokoyama, T. Nishihara, and M. Ueda, Appl. Phys. Express **8**, 061501 (2015).

[10] C. Tholander, F. Tasnádi, I. A. Abrikosov, L. Hultman, J. Birch, and B. Alling, Phys. Rev. B **92**, 174119 (2015).

[11] M. Uehara, H. Shigemoto, Y. Fujio, T. Nagase, Y. Aida, K. Umeda, and M. Akiyama, Appl. Phys. Lett. **111**, 112901 (2017).

[12] S. A. Anggraini, M. Uehara, H. Yamada, and M. Akiyama, Scr. Mater. **159**, 9 (2019).

[13] S. A. Anggraini, M. Uehara, K. Hirata, H. Yamada, and M. Akiyama, Mater. Chem. Phys. **276**, 125394 (2022).

[14] H. H. Nguyen, H. Oguchi, L. Van Minh, and H. Kuwano, "Development of a lead-free piezoelectric (Mg,Hf) co-doped Aln thin film surpassing Pzt in vibration energy harvester performance," unpublished (2024); available at https://dx.doi.org/10.2139/ssrn.4704942.

[15] S. A. Anggraini, M. Uehara, H. Yamada, and M. Akiyama, Mater. Lett. **219**, 247 (2018).

[16] S. A. Anggraini, M. Uehara, K. Hirata, H. Yamada, and M. Akiyama, Sci. Rep. **10**, 4369 (2020).

[17] M. Akiyama, T. Kamohara, K. Kano, A. Teshigahara, and N. Kawahara, Appl. Phys. Lett. **93**, 021903 (2008).

[18] M. R. Islam, N. Wolff, G. Schönweger, T.-N. Kreutzer, M. Brown, M. Gremmel, P. Stráňák, L. Kirste, G. L. Brennecka, S. Fichtner, and L. Kienle, Improved leakage currents and polarity control through oxygen incorporation in ferroelectric $Al_{0.73}Sc_{0.27}N$ thin films," arXiv:2411.17360 [physics]. (2024).

[19] I. Drury and E. Daniel, *Toward High Operating Temperature AlN-Based Ferroelectric Random Access Memory* (Geoffrey Brennecka, 2023).

[20] J. Startt, M. Quazi, P. Sharma, I. Vazquez, A. Poudyal, N. Jackson, and R. Dingreville, Adv. Electron. Mater. **9**, 2201187 (2023).

[21] K. Yazawa, D. Drury, A. Zakutayev, and G. L. Brennecka, Appl. Phys. Lett. **118**, 162903 (2021).

[22] D. Drury, K. Yazawa, A. Mis, K. Talley, A. Zakutayev, and G. L. Brennecka, Phys. Status Solidi RRL **15**, 2100043 (2021).

[23] R. Nie, S. Shao, Z. Luo, X. Kang, and T. Wu, Micromachines **13**, 1629 (2022).

[24] A. Suceava, J. Hayden, K. P. Kelley, Y. Xiong, B. Fazlioglu-Yalcin, I. Dabo, S. Trolier-McKinstry, J.-P. Maria, and V. Gopalan, Opt. Mater. Express **13**, 1522 (2023).

[25] M. Müller, P. Lömker, P. Rosenberger, M. Hussein Hamed, D. N. Mueller, R. A. Heinen, T. Szyjka, and L. Baumgarten, J. Vac. Sci. Technol. A **40**, 013215 (2022).

[26] O. Rehm, L. Baumgarten, R. Guido, P. M. Düring, A. Gloskovskii, C. Schlueter, T. Mikolajick, U. Schroeder, and M. Müller, Phys. Status Solidi RRL **19**, 2400307 (2024).

[27] C.-W. Lee, R. W. Smaha, G. L. Brennecka, N. Haegel, P. Gorai, and K. Yazawa, "From prediction to experimental realization of ferroelectric wurtzite $Al_{1-x}Gd_xN$ alloys," arXiv:2407.11262 [cond-mat]. (2024).

[28] C.-W. Lee, K. Yazawa, A. Zakutayev, G. L. Brennecka, and P. Gorai, Sci. Adv. **10**, eadl0848 (2024).

[29] K. Yazawa, J. S. Mangum, P. Gorai, G. L. Brennecka, and A. Zakutayev, J. Mater. Chem. C **10**, 17557 (2022).

[30] D. Wang, P. Wang, B. Wang, and Z. Mi, Appl. Phys. Lett. **119**, 111902 (2021).

[31] G. Schönweger, A. Petraru, M. R. Islam, N. Wolff, B. Haas, A. Hammud, C. Koch, L. Kienle, H. Kohlstedt, and S. Fichtner, Adv. Funct. Mater. **32**, 2109632 (2022).

[32] O. Ambacher, B. Christian, N. Feil, D. F. Urban, C. Elsässer, M. Prescher, and L. Kirste, J. Appl. Phys. **130**, 045102 (2021).

[33] S. Sivaramakrishnan, P. Mardilovich, T. Schmitz-Kempen, and S. Tiedke, J. Appl. Phys. **123**, 014103 (2018).

[34] J. F. Scott, Integr. Ferroelectr. **12**, 71 (1996).

[35] D. Zhuang and J. Edgar, Mater. Sci. Eng., R **48**, 1 (2005).